Impact damage in woven carbon fibre/epoxy laminates: Analysis of damage and dynamic strain fields

Available online at www.sciencedirect.com

ScienceDirect

Procedia Engineering 199 (2017) 2500–2505

Procedia Engineering

www.elsevier.com/locate/procedia

X International Conference on Structural Dynamics, EURODYN 2017

Impact damage in woven carbon fibre/epoxy laminates: analysis of damage and dynamic strain fields

Laurence A. Coles[a], Anish Roy[a], Leonid Voronov[b], Sergey Semenov[b,*], Mikhail Nikhamkin[b], Nickolay Sazhenkov[b], Vadim V. Silberschmidt[a]

[a]*Wolfson School of Mechanical and Manufacturing Engineering, Loughborough University, Leicestershire, LE11 3TU, UK*
[b]*Aircraft Engines Department, Perm National Research Polytechnical University, Komsomolsky prosp., 29, 614000, Perm, Russian Federation*

Abstract

In this study the resultant ballistic dynamic response observed in a 2x2 twill weave T300 carbon fibre/epoxy composite flat-plate specimen is examined, using a combination of non-invasive analysis techniques. The study investigates deformation and damage caused by impacts of two types of projectiles: solid (steel) travelling with velocity of 70-90 m/s, and fragmenting (ice) with the velocity in the range of 300-500 m/s. Digital image correlation was employed to obtain displacement and to estimate dynamic strain fields from the rear surfaces of the specimens during each experiment. 3D X-ray computer tomography (CT) was used to image and visualize the resultant damage inside the samples. It was shown that solid projectiles lead to greater localized deformation and in some cases penetration, whereas fragmenting projects destroyed on impact cause a more distributed impact load but can lead to major front-surface damage depending on the depth of indentation before fragmentation.

Peer-review under responsibility of the organizing committee of EURODYN 2017.

Keywords: Ballistic Impact, CFRP, X-ray Tomography, Deformation, Damage, Digital image correlation

1. Introduction

Over the last few decades, the use of fibre-reinforced composites (FRCs) has risen considerably across many areas of application including automotive, aerospace, naval, defence, energy and sport. Service conditions of all these areas can include dynamic loading events, resulting in minor or major damage to components or structures. Some examples of typical dynamic loading may include: low- and high-velocity impacts (1 to 1000 m/s) ranging

* Corresponding author. Tel.: +7-919-494-8392
E-mail address: sergey.semyonov@mail.ru

1877-7058
Peer-review under responsibility of the organizing committee of EURODYN 2017.
10.1016/j.proeng.2017.09.420

from flight at Mach 1-2 (300-600 m/s) of fast jets or intercontinental ballistic missiles through clouds of airborne debris or hailstone, to lower-velocity events caused by debris on runways, railway lines, automotive race tracks etc. As a result, it becomes increasingly important to fully understand the effect of various dynamic loading conditions on a FRC's response, in terms of both local and global deformation as well as visible and hidden damage.

The last decade has seen a vast amount of research effort towards characterising the response of FRC's to various dynamic loading conditions, but drawing comparisons between these studies is challenging and often impossible due to their major differences such as type of specimens and, more importantly, experimental and analytical methodologies. In the past, some papers tried to surmise an overview of, for example, impact behaviour [1, 2], but given a breadth of experimental data drew mostly qualitative conclusions regarding the effects of differences in methodology, specimen as well as projectile mass and velocity on such features as delamination behaviour.

An important aspect of this dynamic study is understanding the types of loading conditions and their effect on the specimen over time. For instance, a large part of both experimental and numerical studies was focused on the resulting deformation and damage caused by solid (typically steel) projectiles. In recent years, efforts were made to understand the impact process of ice projectiles [3] and the effect of their fragmentation on composite specimens as well as distribution of load and dispersion of kinetic energy [4, 5]. But, typically, the analysis of the induced damage is limited to a visual inspection of external surfaces, or a use of invasive techniques to study internal damage; the latter could introduce unwanted damage complicating the analysis [6-10]. Some studies employed X-ray tomography to investigate damage [11]. Other new technologies, such as digit image correlation method, were also applied [12].

This paper presents the experimental case studies of ballistic impacts of carbon fibre/epoxy specimens with steel and ice projectiles, using digital image correlation and X-ray computed tomography (CT) to investigate and compare the levels of deformation and damage.

2. Experimental Setup

2.1. Materials and Specimens

The tested carbon-fibre-reinforced/epoxy specimens, measuring approximately 195 mm x 195 mm with a thickness of 5.6 mm were fabricated from 10 plies of carbon-fibre fabric, pre-impregnated with a toughened epoxy matrix (IMP530R). The 10 plies were formed to a laminate consisting of 2 surface plies (T300 3K) and 8 central bulking plies (T300 12K), with a 0°/90° layup configuration, with a theoretical density of 1600 kg/m3. All specimens were manufacture using the autoclave process, cured at 120°C with a 1.5°C per minute ramp rate and a soak time of 160 minutes at a pressure of 90 psi under full vacuum.

2.2. Pneumatic Gun and Specimen Setup

The investigation was performed on a specially developed ballistic experimental apparatus utilising a pneumatic gun (Figure 1). Carbon fiber reinforced polymer (CFRP) specimens were installed into a 4-axis positioning system, and aligned with the barrel resulting in a cantilever clamping scheme, with all specimens being subjected to a orthogonal impact (as shown in Figure 2). The projectile was accelerated to the required speed in the barrel using compressed air, and muzzle velocity measurements were collected using a light gate device installed between the specimen and the end of barrel. Projectile velocities were then determined by the time difference between the signal peaks from the light gates; the experiment was controlled by a PC via a PXI system (National Instruments). The impact process was captured using two high-speed cameras (Photron Fastcam SA5) configured in two arrangements, the first of which captured the front and top views at 25,000 - 50,000 frames per second while the second recorder the rear surface for digital image correlation (DIC) using the VIC-3D (Correlated Solutions) system at 60,000 frames per second. Following parameters of digital image correlation method where defined during pilot experiments : local area subset 15x15 px, step 2 px.

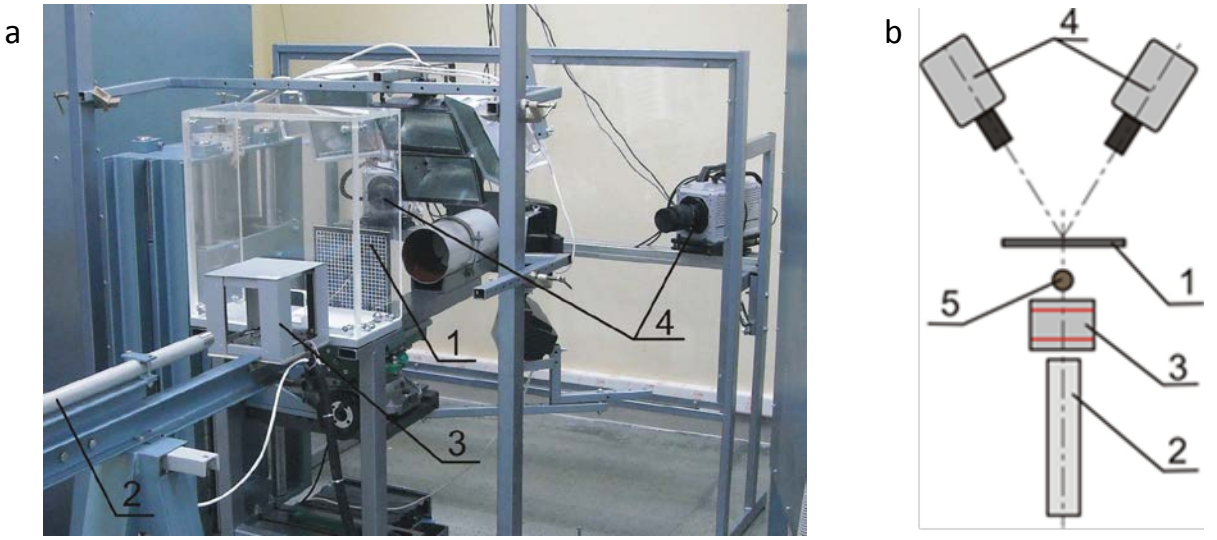

Fig. 1. Appearance of test rig (a) and camera positioning scheme (b, view from the top) for dynamic strain fields investigation. 1 – the specimen, 2 – pneumatic gun, 3 – speed measurement device, 4 – high speed cameras, 5 – the projectile

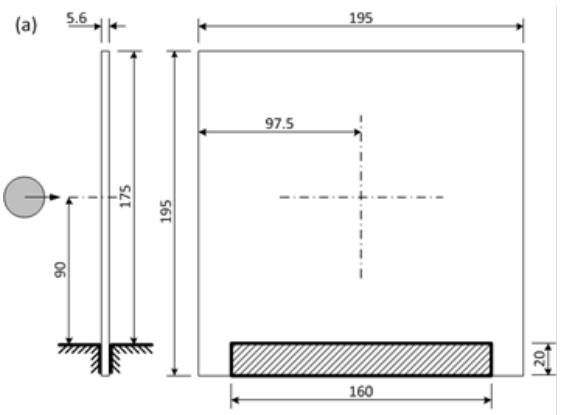

ddFig. 2. Ballistic impact regime and cantilever clamping fixture

2.3. Projectile and Experiment Parameters

All the solid (steel) projectiles were measured to be 23.8 mm diameter with a weight of 54.7 g, and the fragmenting ice (hailstone imitation) projectiles had a diameter 25 mm with a weight of 7.5 g at a temperature of -20°C. The impact velocities were chosen so to produce three levels of damage in the specimens – minor, medium and major with penetration, and were determined during calibration experiments to correspond to approximately 60, 75 and 90 m/s for the steel projectiles and 300, 400 and 500 m/s for the ice ones.

2.4. Configuration of X-Ray Tomography Scans

All of the specimens were inspected using a Metris 160 H-XT X-ray micro CT system to investigate the extent of the internal damage and its spatial distribution. Each scan was conducted at 140 kV and 130 μA using a tungsten target, with 2650 radiography projections taken over the 360° rotation for each specimen at an exposure of 500 ms.

In order to reduce granular noise, 8 images where taken and averaged per projection. The total volume scanned for each specimen was 180 mm x 140 mm x 20 mm at a resolution of 97 μm.

3. Experimental results and discussion

Typical impacts with both the steel and ice projectiles in the experimental studies can be seen in Figure 3, where the ice projectile initially indented the specimen before fragmenting within it, causing major wide-spread delamination of the first few plies. The impact with the steel projectile resulted in major indentation before full penetration, as expected, inducing more localised damage when compared to that of the ice projectiles.

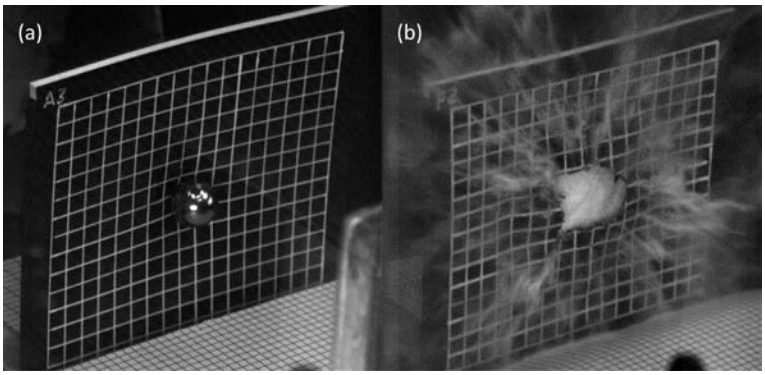

Fig. 3. Typical impact behavior of solid steel projectile at 0.40 ms (speed – 78.1 m/s) (a) and fragmenting ice projectile at 0.19 ms (speed – 480 m/s) (b)

3.1. Deformation Analysis

Analysing impacts with the steel projectile in terms of global displacement, it is clear that due to the more rigid nature of the material, the composite demonstrated more defined indentation before the transition into global flexural bending. For the ice projectiles this initial indentation was still present, but upon fragmentation this local indentation was more gradually transitioned due to the distributed load, leading to global flexural bending. This difference in the distribution of dynamic loads led to varying curvature of the specimen during loading. For the solid projectiles the curvature was small, with transitions between concave and convex forms happening gradually, whereas for the ice projectile this transition was more abrupt and resulted multiple damage modes. As the ice fragmented on impact, the local indentation of the specimen became more widespread causing a more distributed loading and, hence, reduced failure at the rear surface. In the case of the solid projectile, this damage occurred much sooner.

From localized deformation behavior and the normalized response of each specimen, it became evident that the maximum out-of-plane displacement increased with the growing impact velocity (energy). The time until maximum displacement reduced with the increased velocities (energies), although this trend was not as clear due to the limitation related to time resolution (directly linked to the frame rate of the used camera).

There where dynamic strain fields obtained with digital image correlation system on the rear surface of the specimen during impact loading. The example of the strain field ε_{yy} are shown in Figure 4 for ice projectile impact with 300 m/s velocity. It can be seen, that impact comes with maximal stretching ε_{yy} =0.94% in the central part of the specimen with size 60 mm and maximal compression ε_{yy} =- 0.31% at periphery.

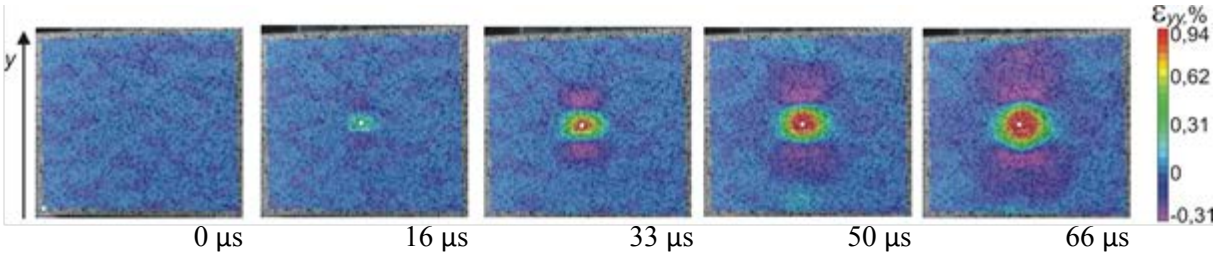

Fig. 4. Example of strain field distribution (εyy) on the back surface of specimen at different points in time, DIC

3.2. Damage Analysis

Inspections the specimens after ballistic impact tests with the solid (steel) and fragmenting (ice) projectiles demonstrated two very distinct types of visual damage: (a) highly localized and, therefore, more penetrating damage from the steel projectiles and (b) more widespread damage to the front surface of the specimen with some signs leading to the early stages of penetration in the case of the ice projectiles. Figure 5 shows the damage clouds for two major damage loading conditions. From the results of the CT scans it is clear that the main damage modes were delamination (darker zones) and tensile fibre damage, but at the employed resolution it was not possible to accurately determine any other damage mechanisms.

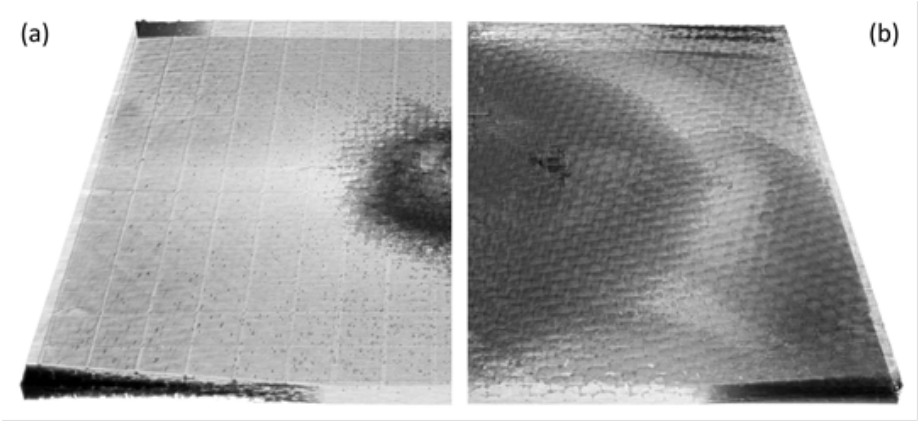

Fig. 5. Typical examples of internal damage cloud in composite specimens caused by solid (steel speed – 78.1 m/s) (a) and fragmenting ice (speed – 480 m/s) (b) projectiles (the darker zone the lower integrity of zone)

This was confirmed for all the three damage modes for both types of the projectiles by analysis of other 3D views: for the steel projectile, the damage cloud remained highly localised even under increasing energy whereas for the ice projectile it increased more clearly.

The transparent 3D tomograms allowed assessment of the damage areas and greyscale intensity, with the latter being related to the extent of damage accumulation through the thickness of the specimen. For instance, the specimen impacted with the solid projectile demonstrated a dark-grey zone toward the centre, indicating greater damage like penetration, whereas the fragmenting projectiles caused catastrophic damage across the whole front surface and first few plies of the composite target, causing a more distributed gradient of the intensity.

4. Conclusions

For impacts with projectiles of the same size, a case with the solid (steel) ones demonstrated more defined indentation of the specimens before the transition to global flexural bending, whereas fragmenting (ice) projectiles produced initial indentation that, upon fragmentation, more gradually transitioned to distributed loading leading to

global flexural bending. Comparing each of the loading conditions showed that projectiles of the same material will produce similar responses of the impacted specimen, even at different energy levels. Oppositely, two projectiles of different materials will show different levels of indentation within the specimen, even at lower energy levels. The character of transition from indentation to global flexural bending also changed with projectile material, affecting the evolution of specimen's curvature during its deformation.

Damage at the rear surface of the specimens occurred much sooner in the case of the solid projectile; this is likely due to the almost instantaneous fragmentation of the ice projectile on impact causing a broader distribution of impact load and, therefore, a longer impact duration even at clearly higher impact energies. Although the fragmenting projectile did mitigate the penetration of the specimen, the partial indentation followed by the projectile's destruction, causing delamination and removal of the first 2-3 plies from the front surface of the impacted composite plate.

Strain field analysis for experiments with ice-projectile shown the presence of stretching areas at the impact point with size up to 60 mm and maximum strain values up to 1.08% and compression zones with strain values down to –0.31% at 40 mm distance from impact point.

The following work is supposed to be continued in two directions: improving of damage mechanism understanding using tomography with better resolution and numerical simulation of specimen damaging process.

References

[1] Abrate, S. Impact on laminated composites. ASME: Applied Mechanics Reviews, 44:155-190, 1991.
[2] Abrate, S. Impact on laminated composites: Recent advances. Composites. ASME: Applied Mechanics Reviews, 47:517-544, 1994.
[3] Pernas-Sánchez, J. Artero-Guerrero, J.A, Varas, D., López-Puente, J. Analysis of ice impact process at high velocity. Experimental Mechanics, 55:1669-1679, 2015.
[4] Kim, H., Welch D.A., Kedward, K.T. Experimental investigation of high velocity ice impacts on woven carbon/epoxy composite panels. Composites Part A: Applied Science and Manufacturing, 34:25-41, 2003.
[5] Appleby-Thomas, G.J., Hazell, P. J., Dahini, G. On the response of two commercially-important CFRP structures to multiple ice impacts. Composite Structures, 93:2619-2627, 2011.
[6] Nunes, L.M., Paciornik, S., d'Almeida, J.R.M. Evaluation of the damaged area of glass-fiber-reinforced epoxy-matrix composite materials submitted to ballistic impacts. Composites Science and Technology, 64: 945-954, 2004.
[7] Sevkat, E. Experimental and numerical approaches for estimating ballistic limit velocities of woven composite beams. International Journal of Impact Engineering. 45: 16-27, 2012.
[8] Shaktivesh, N.S. Nair, Ch.V. Kumar, S., Naik, N.K. Ballistic impact performance of composite targets. Materials & Design. 51: 833-846, 2013.
[9] Pandya, K.S., Pothnis, J.R., Ravikumar, G., Naik, N.K. Ballistic impact behavior of hybrid composites. Materials & Design. 44: 128-135, 2013.
[10] Yahaya, R., Sapuan, S.M., Jawaid, M., Leman, Z., Zainudin, E.S. Quasi-static penetration and ballistic properties of kenaf–aramid hybrid composites. Materials & Design. 63: 775-782, 2014.
[11] Karthikeyan, K., Russell, B.P., Fleck, N.A., Wadley, H.N.G., Deshpande V.S. The effect of shear strength on the ballistic response of laminated composite plates. European Journal of Mechanics - A/Solids. 42: 35-53, 2013.
[12] Nikhamkin M.Sh., Voronov L.V., Bolotov B.P. Experimental finding of dynamic deformation fields in metal and composite plates under impact. PNRPU Mechanics Bulletin 2 (2015) 103-115.